International Journal of Heat and Mass Transfer 149 (2020) 119184

Contents lists available at ScienceDirect

International Journal of Heat and Mass Transfer

journal homepage: www.elsevier.com/locate/hmt

Melting behavior of phase change materials in the presence of a non-uniform magnetic-field due to two variable magnetic sources

S.A.M. Mehryan[a], Ali Tahmasebi[b], Mohsen Izadi[c], Mohammad Ghalambaz[d,e,*]

[a] Young Researchers and Elite Club, Yasooj Branch, Islamic Azad University, Yasooj, Iran
[b] Department of Mechanical Engineering, Shahid Chamran University of Ahvaz, Ahvaz, Iran
[c] Mechanical Engineering Department, Faculty of Engineering, Lorestan University, Khorramabad, Iran
[d] Department for Management of Science and Technology Development, Ton Duc Thang University, Ho Chi Minh City, Vietnam
[e] Faculty of Applied Sciences, Ton Duc Thang University, Ho Chi Minh City, Vietnam

ARTICLE INFO

Article history:
Received 24 August 2019
Revised 17 November 2019
Accepted 7 December 2019
Available online 16 December 2019

Keywords:
Phase change materials (PCMs)
Non-magnetic-field
Arbitrary Lagrangian-Eulerian (ALE)
Melting front

ABSTRACT

A uniform melting of a metal or polymer is essential for the quality of products. In a melting process, the convection flows affect the heat transfer, and result in a non-uniform melting process. The presence of a magnetic-field can control the flow and heat transfer by Lorentz and Kelvin forces. The present study aims to analyze the effect of the presence of two magnetic sources on the melting flow and heat transfer in a cavity. Here, the process of heat absorption by the PCM-filled enclosure that is exposed to two non-uniform magnetic-fields is numerically studied. The strengths of two magnetic-fields are not necessarily the same. Tracking the interface of solid and fluid portions of phase change material is performed using the deformed mesh technique. Galerkin finite element method, along with the Arbitrary Lagrangian-Eulerian is applied to solve the characteristic equations. The results show that the progress of the melting front completely depends on the intensity ratio of two non-uniform magnetic-fields γ_r. Besides, although the magnetic number has a slight effect on the melting, an increase in Hartman number can drastically decline the progress of the melting front.

1. Introduction

The melting heat transfer is an essential part of various industrial applications such as the melting of metals for metal casting, melting of polymer solutions for 3D printing, melting of glass or plastics for molding. In practice, the uniform melting of materials in the containers significantly influences the quality of the molten solution and the final product. One of the parameters which induce a non-uniform melting interface in an enclosure is the buoyancy effects in the molten solution. The buoyancy forces induce a flowing movement and convective heat transfer. The regions, exposed to a strong flow movement, experience a higher rate of heat transfer and melt faster. Thus, methods capable of controlling the melting process are of much interest.

The presence of a magnetic-field is one way of controlling the flow and consequently the heat transfer in an enclosure [1]. In this regard, there is a substantial amount of researches, which investigated the natural convection heat transfer in an enclosure in the presence of a uniform magnetic-field. For instance, Dogonchi et al. [2] explored the influence of a uniform inclined magnetic-field on the thermal behavior of the fluid in a porous space between two cylinders. Umavathi et al. [3] considered a vertical channel subject to a uniform magnetic-field. These researchers addressed the effect Magneto-HydroDynamic (MHD) effects on the flow behavior in the channel. Ma et al. [4] explored the influence of an inclined and uniform magnetic-field on the thermal behaviours of nanofluids in a U shape enclosure. They reported that the presence of the magnetic-field suppresses the flow and reduces the heat transfer rate in the enclosure. They also revealed that the influence of the magnetic-field on heat transfer is more significant when the natural convection effects are strong.

Alsabery et al. examined the influence of an inclined and uniform magnetic-field on the conjugate free convection flow and heat transfer in an enclosure. They found that the elevation of the magnetic-field strenght suppresses the convective flow and heat transfer in the enclosure. Gibanov et al. [5] modeled the natural convection heat transfer in a cavity enclosure, which was partially filled with two types of porous media. The cavity was exposed to an inclined magnetic-field. The results show that the porous medium and magnetic-field could notably control the flow and heat transfer in the cavity. The effect of a uniform magnetic-field

* Corresponding author at: Ton Duc Thang University, Ho Chi Minh City, Vietnam
E-mail address: mohammad.ghalambaz@tdtu.edu.vn (M. Ghalambaz).

https://doi.org/10.1016/j.ijheatmasstransfer.2019.119184
0017-9310/

on various aspect of natural convection heat transfer in enclosures including ferrofluids [6], conjugate heat transfer in porous media [7], hybrid nanofluids [8], thermal radiation [9], and periodic uniform magnetic-field [10] are also addressed.

The control of heat transfer in a boundary by a uniform magnetic-field is another aspect of MHD flows. In this regard, Chamkha et al. [11] addressed natural convection and heat transfer of a binary fluid over a vertical cylinder. Chamkha and Rashad [12] investigated the influence of a uniform magnetic-field on the concentration gradient of a binary fluid over a rotating cone. Later, Mallikarjuna et al. [13] examined the influence of the uniform magnetic-field on the thermal behavior of a fluid with a chemical reaction.

The phase change materials (PCMs) are a type of substance, which can store/release a substantial amount of energy on phase change between a solid and liquid state in the form of the latent heat. PCMs are of interest to various practices in energy storage and thermal management systems. For example, Sadeghi et al. explored the effect of using a multi-layer of PCM in a tubular heat exchanger. Boukani et al. [14] studied the influence of nano-additives on the phase change heat transfer in an elliptical capsule. The outcomes show that melting heat transfer in an elliptical capsule is better than a circular capsule. Moreover, using nanoparticles increases the melting rate, but it reduces the amount of phase change material in the capsule. The phase change materials for electronic heatsinks [15, 16] are also investigated. There are also some recent studies on the natural/mixed convection heat transfer of nano-encapsulated phase change materials in the clear flow [17, 18] and porous media [17]. The non-Newtonian phase change heat transfer in a vertical symmetrical enclosure is examined by Ghalambaz et al. [19] while there was a partial layer of a porous medium in the enclosure. The results show that the presence of a pseudoplastic non-Newtonian behavior improves the natural convection and melting rate in the enclosure.

Regarding the uniform magnetic-field and phase change, there are only a few studies available. Farsani et al. [20] explored the effect of a uniform magnetic-field on the melting of Gallium in a rectangular cavity. The results show that the rise of magnetic-field intensity reduces the flow movement and heat transfer in the melting region of the cavity. Sheikholeslami and Mahian [21] and Sheikholeslami [22] investigated the phase change heat transfer of nano-enhanced water (CuO-water) filled in a porous medium. They investigated two geometries of the space between two pipes [21] and the geometry of the space between two ducts with unregular shape [22]. They reported that the increase of the magnetic strength increases the required time for phase change of the CuO-water from liquid to solid. Selimefendigil et al. [23] addressed the phase change heat transfer of PCMs in an enclosure-cavity exposed to an inclined magnetic-field. They reported a slight change of heat transfer by changing the inclination angle of the magnetic-field.

In all of the studies mentioned so far, the magnetic-field was uniform in space. However, in most of the practical cases, the magnetic-field is not uniform in space. For instance, the magnetic-field about a solenoid or an electrical wire is not uniform in space. Only a few recent studies investigated the effect of a non-uniform magnetic-field on the flow and heat transfer in an enclosure. Sheikholeslami and Vajravelu [24] investigated the influence of the presence of a point source on the natural convection heat transfer in an enclosure heated from below. The influence of the variable magnetic-field, on the natural convection flows, is also investigated in the works of Izadi et al. [25], Sheikholeslami et al. [26], Sheikholeslami and Rokni [27] and Sheikholeslami and Mohadeseh [28]. In all of these studies with the variable magnetic-field, it was assumed that the enclosure is filled with a molten fluid, and there is no phase change.

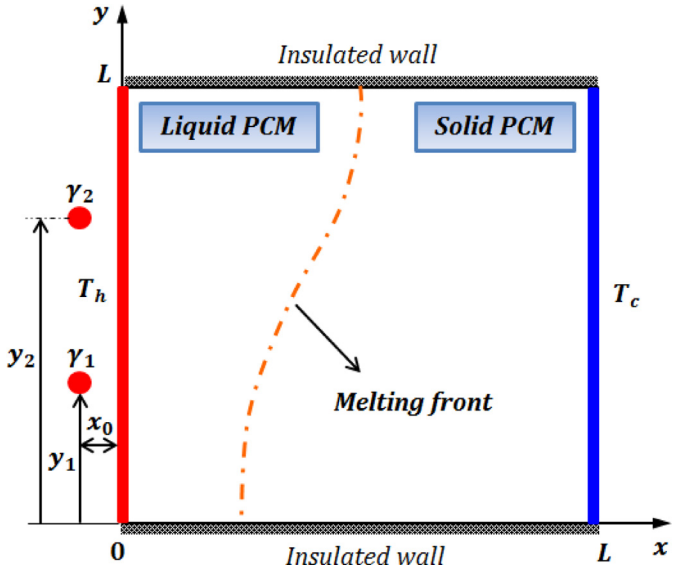

Fig. 1. Schematic view of the physical model and coordinate system.

In very recent study, Ghalambaz et al. [29] addressed the melting phase change in the presence of a magnetic-field originated from a concentrated source. The results show that a focused magnetic source can provide a notable effect on the final stages of the melting process. Following [29], the present study aims to address the melting behavior of a phase change material in a square enclosure in the presence of two variable magnetic-fields using a moving grid method for the first time.

2. Problem definition and formulation

Fig. 1 represents a schematic of the studied subject and its boundary conditions. Here, the simulation of a two-dimensional square cavity is examined that is filled with melting phase-changing material. The temperatures of the left and right side walls are kept at T_h and T_c ($T_h > T_c$). The top and bottom side walls are adiabatic. The melted PCM flow regime is laminar and Newtonian. The entire cavity is exposed to two non-uniform magnetic-fields. The locations of the two sources [(x_0, y_1), (x_0, y_2)] are specified in the figure. Magnetic intensities related to source #1 and #2 are γ_1 and γ_2, respectively. Magnetic-field intensity is inversely proportional to the squared distance from the sources. Magnetic-field vector is defined using the following relations [24, 26]:

$$\boldsymbol{H}_1^* = H_{1x}^* i + H_{1y}^* j = \frac{\gamma_1}{2\pi}\frac{(y-y_1)}{(x-x_0)^2+(y-y_1)^2} i - \frac{\gamma_1}{2\pi}\frac{(x-x_0)}{(x-x_0)^2+(y-y_1)^2} j$$
$$\boldsymbol{H}_2^* = H_{2x}^* i + H_{2y}^* j = \frac{\gamma_2}{2\pi}\frac{(y-y_2)}{(x-x_0)^2+(y-y_2)^2} i - \frac{\gamma_2}{2\pi}\frac{(x-x_0)}{(x-x_0)^2+(y-y_2)^2} j \quad (1)$$

The resultant of the two magnetic-fields are as follows:

$$\boldsymbol{H}^* = \boldsymbol{H}_1^* + \boldsymbol{H}_2^* = H_x^* i + H_y^* j, H^* = \left(H_x^{*^2} + H_y^{*^2}\right)^{0.5} \quad (2)$$

Applying the above-mentioned presumptions and the forces applied to the fluid particles, the following characteristic equations can represent the physics of the phenomena:

Continuity equation:

$$\nabla \cdot \boldsymbol{u} = 0 \quad (3)$$

Momentum equation:

$$\rho\left(\frac{\partial \boldsymbol{u}}{\partial t} + \boldsymbol{u}\cdot\nabla\boldsymbol{u}\right) = -\nabla p + \mu\nabla^2\boldsymbol{u} + \boldsymbol{F} \quad (4)$$

where **F** is the resultant of the following forces:

$$\boldsymbol{F} = \boldsymbol{F_L} + \boldsymbol{F_B} + \boldsymbol{F_K} \tag{5}$$

$\mathbf{F_L}$, known as Lorentz force, is defined as $\mathbf{F_L}$=**J** × **B**. In this relation, **B** is the magnetic induction vector that has the components of $B_x = \mu_0 H_x^*$ and $B_y = \mu_0 H_y^*$. **J** is the voltage field. The vector relation between the magnetic induction and voltage vectors is defined with the following expression:

$$\boldsymbol{J} = \sigma(-\nabla\phi + \boldsymbol{u} \times \boldsymbol{B}) \tag{6}$$

$\mathbf{F_k}$, which is known as the Kelvin force, results from the magnetic-field variations. Its components in the x and y directions are represented as $\mu_0 M \partial H^*/\partial x$ and $\mu_0 M \partial H^*/\partial y$. M is called magnetization and is defined using the following experimental relation.

$$M = K' H^* \left(T'_C - T\right) \tag{7}$$

Finally, $\mathbf{F_B}$ represents the buoyancy force employed to the fluid that is defined as

$$\boldsymbol{F_B} = \beta \rho g \left(T - T_f\right) \tag{8}$$

In the deformed mesh approach, the energy equation in the liquid and solid PCM are written independently and then they will be connected using the interface energy balance (Stephan condition). Hence, the energy equations in the liquid and solid parts of the domain are written as:

The energy equation for the liquid PCM:

$$(\rho C_p)_l \left(\frac{\partial T}{\partial t} + \boldsymbol{u} \cdot \nabla T\right) = k_l \nabla^2 T + Q \tag{9}$$

Q, heat generation due to presence and variations of the magnetic-field, is modeled using the following relation.

$$Q = Q_J + Q_M \tag{10}$$

where Q_J is Joule heating resulting from the presence of the magnetic-field and electrical conductivity of the liquid PCM. It is defined as:

$$Q_J = \sigma (u B_y - v B_x)^2 \tag{11}$$

In physics, eddy current (French: Courants de Foucault) are referred to circular and scattered electric currents that are induced in a conductor by a time-varying magnetic-field. The variability of this magnetic-field can be due to an alternating current, or the relative motion between the conductor and magnetic-field. When a conductor is exposed to variation of a magnetic-field due to the relative motion of the conductor and field source, or to the variation of the field itself due to an alternating current, scattered (eddy) circulating currents occur in the conductor (induced current). These eddy currents, in turn, produce magnetic-fields that oppose the change in the primary magnetic-field, according to the lens law, thereby generating repulsive and attractive forces between the conductor and the magnet. The term eddy current is derived from similar currents in the water. These currents occur when paddling in the water. The turbulence localized areas, called vorticities, occur in continuous vorticities. Eddy currents, such as electric current, generate heat and magnetic force. This heat can be used for induction heating. Eddy currents are also the cause of levitation in superconductors and can have undesirable effects, including power loss in converters and transformers. Laminating the conductors minimizes these losses. Magnetocaloric effects are due to the variations and gradient of the magnetic-field, which is represented as:

$$Q_M = \mu_0 T \frac{\partial M}{\partial T}\left(u\frac{\partial H^*}{\partial x} + v\frac{\partial H^*}{\partial y}\right) \tag{12}$$

The thermodynamics can well explain the basis of the magnetocaloric effect (MCE). Magnetic variables can be related to temperature and entropy using MCE. The coupling of magnetic sublattice to the external magnetic-field, which can modify the magnetic contribution to the entropy, is known as the basis of MCE. An increase or decrease in the strength of an external magnetic-field modifies the ordering of the magnetic moments of the atoms forming the material, thus shifting magnetic entropy. Regarding the thermodynamics analogous, the isothermal compression of a gas is equivalent to the isothermal magnetization of a magnetizable material. In fact, applying pressure results in the entropy reduction when the temperature is kept to be constant. On the other hand, the adiabatic expansion of gas during a total constant entropy process, which yields a decrease in temperature is similar to adiabatic demagnetization. The total entropy remains constant, and temperature declines while removing the applied magnetic-field because the magmatic entropy augments.

The energy equation for solid PCM:

$$(\rho C_p)_s \frac{\partial T}{\partial t} = k_s \nabla^2 T \tag{13}$$

Finally, the mentioned characteristic equations are solved using the following boundary conditions.

$$u = v = 0,\ T = T_h \qquad \forall x, y, t | x = 0, 0 \le y \le L, t \ge 0 \tag{14-a}$$

$$u = v = 0,\ T = T_c = 0 \qquad \forall x, y, t | x = L, 0 \le y \le L, t \ge 0 \tag{14-b}$$

$$u = v = 0,\ \frac{\partial T}{\partial y} = 0 \qquad \forall x, y, t | y = 0, 0 \le x \le L, t \ge 0 \tag{14-c}$$

$$u = v = 0,\ \frac{\partial T}{\partial y} = 0 \qquad \forall x, y, t | y = L, 0 \le x \le L, t \ge 0 \tag{14-d}$$

$$u = v = 0, T = T_0 \qquad \forall x, y, t | 0 \le y \le L, 0 \le x \le L\ , t = 0 \tag{14-e}$$

Stefan condition and energy balancing in the melting boundary are applied to estimate the melting rate and numerical mesh relocation:

$$k_l \frac{\partial T}{\partial x}\bigg|_l - k_s \frac{\partial T}{\partial x}\bigg|_s = \rho u h_{sf} \tag{15-a}$$

$$k_l \frac{\partial T}{\partial y}\bigg|_l - k_s \frac{\partial T}{\partial y}\bigg|_s = \rho v h_{sf} \tag{15-b}$$

The following relations are utilized to make the characteristic equations dimensionless:

$$X = \frac{x}{L},\quad Y = \frac{y}{L},\quad U = \frac{uL}{\alpha_l}, V = \frac{vL}{\alpha_l},\quad \theta = \frac{T - T_c}{T_h - T_c},\ P = \frac{L^2 p}{\rho {\alpha_l}^2},$$
$$H = \frac{H^*}{H_0^*},\quad H_X = \frac{H_x^*}{H_0^*},\quad H_Y = \frac{H_y^*}{H_0^*}, Fo = \frac{t\alpha_l}{L^2} \tag{16}$$

where $H_0^* = \gamma_1/2\pi L$. Using the dimensionless relations (16), the characteristic equations are transformed into their final dimensionless forms.

$$\frac{\partial U}{\partial X} + \frac{\partial V}{\partial Y} = 0 \tag{17}$$

$$\frac{\partial U}{\partial F_0} + U\frac{\partial U}{\partial X} + V\frac{\partial U}{\partial Y} = -\frac{\partial P}{\partial X} + Pr\left(\frac{\partial^2 U}{\partial X^2} + \frac{\partial^2 U}{\partial Y^2}\right) - Ha^2 Pr H_Y (U H_Y - V H_X) - Mn_f Pr\theta H \frac{\partial H}{\partial X} \tag{18}$$

$$\frac{\partial V}{\partial F_0} + U\frac{\partial V}{\partial X} + V\frac{\partial V}{\partial Y} = -\frac{\partial P}{\partial Y} + Pr\left(\frac{\partial^2 V}{\partial X^2} + \frac{\partial^2 V}{\partial Y^2}\right) + RaPr\theta - Ha^2 Pr H_X (V H_X - U H_Y) - Mn_f Pr\theta H \frac{\partial H}{\partial Y} \tag{19}$$

$$\frac{\partial\theta}{\partial F_0}+U\frac{\partial\theta}{\partial X}+V\frac{\partial\theta}{\partial Y}=\left(\frac{\partial^2\theta}{\partial X^2}+\frac{\partial^2\theta}{\partial Y^2}\right)+EcHa^2(UH_Y-VH_X)^2 \\ +Mn_f EcH(\varepsilon_1+\theta)\left(U\frac{\partial H}{\partial X}+V\frac{\partial H}{\partial Y}\right) \tag{20}$$

$$\frac{(\rho C_p)_s}{(\rho C_p)_l}\frac{\partial\theta}{\partial F_0}=\frac{k_s}{k_l}\left(\frac{\partial^2\theta}{\partial X^2}+\frac{\partial^2\theta}{\partial Y^2}\right) \tag{21}$$

As it is seen, the dimensionless numbers play an important role in the appeared equations, which will be discussed.

$$Ra=\frac{g\beta\Delta TL^3}{\mu_l\alpha_l},\ Pr=\frac{\upsilon}{\alpha_l},\ Ha=\mu_0H_0^*L\sqrt{\frac{\sigma_l}{\mu_l}}, \\ Ec=\frac{\mu_l\alpha_l}{\rho C_p\Delta TL^2},\ Mn_f=\frac{\mu_0H_0^{*^2}K'\Delta TL^2}{\mu_l\alpha_l} \tag{22}$$

Moreover, the magnetic-field components can be dimensionless as follows

$$H_X=\frac{(Y-Y_1)}{(X-X_1)^2+(Y-Y_1)^2}+\gamma_r\frac{(Y-Y_2)}{(X-X_1)^2+(Y-Y_2)^2} \\ H_Y=-\frac{(X-X_1)}{(X-X_1)^2+(Y-Y_1)^2}-\gamma_r\frac{(X-X_1)}{(X-X_1)^2+(Y-Y_2)^2} \tag{23}$$

where $\gamma_r=\gamma_2/\gamma_1$. Also, using the dimensionless variables, the boundary conditions become dimensionless as follows

$$U=V=0,\theta=1\forall X,Y,Fo|X=0,0\le Y\le 1\ ,Fo\ge 0 \tag{24-a}$$

$$U=V=0,\frac{\partial\theta}{\partial Y}=0\forall X,Y,Fo|X=1,0\le Y\le 1\ ,Fo\ge 0 \tag{24-b}$$

$$U=V=0,\frac{\partial\theta}{\partial Y}=0\forall X,Y,Fo|Y=0,0\le X\le 1\ ,Fo\ge 0 \tag{24-c}$$

$$U=V=0,\frac{\partial\theta}{\partial Y}=0\forall X,Y,Fo|Y=1,0\le X\le 1\ ,Fo\ge 0 \tag{24-d}$$

$$U=V=0,\theta=\theta_0\forall X,Y,Fo|0\le Y\le 1,0\le X\le 1\ ,Fo=0 \tag{24-e}$$

Moreover, the dimensionless rate of the melting boundary motion is represented as

$$U=Ste\left(\left.\frac{\partial\theta}{\partial X}\right|_l-\left.\frac{\partial\theta}{\partial X}\right|_s\right) \tag{25-a}$$

$$V=Ste\left(\left.\frac{\partial\theta}{\partial Y}\right|_l-\left.\frac{\partial\theta}{\partial Y}\right|_s\right) \tag{25-b}$$

where Ste is Stefan number and is defined as

$$Ste=\frac{C_{p,l}\left(T_h-T_f\right)}{h_{sf}} \tag{26}$$

3. Numerical approach, grid test, and verification

The usage of a numerical approach to integrating the mentioned drastically non-linear and coupled equations is necessary. The finite element method based on the Galerkin technique is considered to apply the modeling equations. More details can be found in [30–32]. In the momentum equations, the pressure term is eliminated by writing the pressure in the form of a penalty-function, introduced as:

$$P=\chi\left(\frac{\partial U}{\partial X}+\frac{\partial V}{\partial Y}\right) \tag{27}$$

Assuming a very large number for the χ, known as the penalty number, the continuity equation can be satisfied within a good accuracy. Now, the above equation can be substituted in the momentum equations as:

$$\frac{\partial U}{\partial Fo}+U\frac{\partial U}{\partial X}+V\frac{\partial U}{\partial Y}=-\frac{\partial}{\partial X}\left(\chi\left(\frac{\partial U}{\partial X}+\frac{\partial V}{\partial Y}\right)\right)+Pr\left(\frac{\partial^2U}{\partial X^2}+\frac{\partial^2U}{\partial Y^2}\right) \\ -Ha^2PrH_Y(UH_Y-VH_X) \tag{28}$$

$$\frac{\partial V}{\partial Fo}+U\frac{\partial V}{\partial X}+V\frac{\partial V}{\partial Y}=-\frac{\partial}{\partial Y}\left(\chi\left(\frac{\partial U}{\partial X}+\frac{\partial V}{\partial Y}\right)\right)+Pr\left(\frac{\partial^2V}{\partial X^2}+\frac{\partial^2V}{\partial Y^2}\right) \\ -Ha^2PrH_X(VH_X-UH_Y)+RaPr\theta \tag{29}$$

The velocity components in x and y directions along with and the temperature in both liquid and solid regions is expanded using a basis set $\{\xi_k\}_{k=1}^N$ as:

$$U\approx\sum_{k=1}^{N}U_k\xi_k(X,\ Y),V\approx\sum_{k=1}^{N}V_k\xi_k(X,\ Y),\ \theta\approx\sum_{k=1}^{N}\theta_k\xi_k(X,\ Y) \tag{30}$$

Invoking the same basis function for all of the variables, the following residuals relations in a non-linear form are achieved using the Galerkin finite element approach:

$$R_i^1\approx\sum_{k=1}^{N}U_k\int\frac{\partial\xi_k}{\partial Fo}\xi_i dXdY+\sum_{k=1}^{N}U_k\int\left[\left(\sum_{k=1}^{N}U_k\xi_k\right)\frac{\partial\xi_k}{\partial X}+\left(\sum_{k=1}^{N}V_k\xi_k\right)\frac{\partial\xi_k}{\partial Y}\right]\xi_i dXdY \\ +\gamma\left[\sum_{k=1}^{N}U_k\int\frac{\partial\xi_i}{\partial X}\frac{\partial\xi_k}{\partial X}dXdY+\sum_{k=1}^{N}V_k\int\frac{\partial\xi_i}{\partial X}\frac{\partial\xi_k}{\partial Y}dXdY\right] \\ +Pr\sum_{k=1}^{N}U_k\int\left[\frac{\partial\xi_i}{\partial X}\frac{\partial\xi_k}{\partial X}+\frac{\partial\xi_i}{\partial Y}\frac{\partial\xi_k}{\partial Y}\right]dXdY+PrHa^2H_Y^2\int\left(\sum_{k=1}^{N}U_k\xi_k\right)\xi_i dXdY \\ -PrHa^2H_XH_Y\int\left(\sum_{k=1}^{N}V_k\xi_k\right)\xi_i dXdY \tag{31}$$

$$R_i^2\approx\sum_{k=1}^{N}V_k\int\frac{\partial\xi_k}{\partial Fo}\xi_i dXdY+\sum_{k=1}^{N}V_k\int\left[\left(\sum_{k=1}^{N}U_k\xi_k\right)\frac{\partial\xi_k}{\partial X}+\left(\sum_{k=1}^{N}V_k\xi_k\right)\frac{\partial\xi_k}{\partial Y}\right]\xi_i dXdY \\ +\gamma\left[\sum_{k=1}^{N}U_k\int\frac{\partial\xi_i}{\partial Y}\frac{\partial\xi_k}{\partial X}dXdY+\sum_{k=1}^{N}V_k\int\frac{\partial\xi_i}{\partial Y}\frac{\partial\xi_k}{\partial Y}dXdY\right] \\ +Pr\sum_{k=1}^{N}V_k\int\left[\frac{\partial\xi_i}{\partial X}\frac{\partial\xi_k}{\partial X}+\frac{\partial\xi_i}{\partial Y}\frac{\partial\xi_k}{\partial Y}\right]dXdY-RaPr\int\left(\sum_{k=1}^{N}\theta_k\xi_k\right)\xi_i dXdY \\ +PrHa^2H_X^2\int\left(\sum_{k=1}^{N}V_k\xi_k\right)\xi_i dXdY-PrHa^2H_XH_Y\int\left(\sum_{k=1}^{N}U_k\xi_k\right)\xi_i dXdY \tag{32}$$

$$R_i^3\approx\sum_{k=1}^{N}\theta_k\int\frac{\partial\xi_k}{\partial Fo}\xi_i dXdY+\sum_{k=1}^{N}\theta_k\int\left[\left(\sum_{k=1}^{N}U_k\xi_k\right)\frac{\partial\xi_k}{\partial X}+\left(\sum_{k=1}^{N}V_k\xi_k\right)\frac{\partial\xi_k}{\partial Y}\right]\xi_i dXdY \\ +\sum_{k=1}^{N}\theta_k\int\left[\frac{\partial\xi_i}{\partial X}\frac{\partial\xi_k}{\partial X}+\frac{\partial\xi_i}{\partial Y}\frac{\partial\xi_k}{\partial Y}\right]dXdY \\ -EcHa^2\left(H_Y\int\left[\sum_{k=1}^{N}U_k\xi_k\right]-H_X\int\left[\sum_{k=1}^{N}V_k\xi_k\right]\right)^2\xi_i dXdY \tag{33}$$

As it is shown in Table 1, result-independence study is conducted on the generated mesh for Ste = 0.039, Pr = 0.021, Ra = 2.1 × 10^5, Mn_f = 10, Ha = 10, Y_1 = 0.3, Y_2 = 0.7, γ_r = 1, and Ec=10^{-6}. Structured and unstructured meshes with quadratic and triangular elements were used to discretize the calculation domains of liquid and solid PCM phases, respectively. To ensure that the utilized grid size is fine enough to produce accurate outcomes, the results are computed for several grids sizes. The outcomes for the volume fraction of the melted PCM are monitored. Fig. 2 represents the variation of melted PCM fraction versus time for the

Table 1
The details of the mesh sizes in the solid and liquid domains.

Cases	Case 1	Case 2	Case 3	Case 4
Grid size in solid	560	**974**	1412	1868
Grid size in liquid	30 × 30	**60 × 60**	90 × 90	120 × 120
Run time	18 min	**1 h, 9 min**	2 h, 44 min	5 h, 22 min

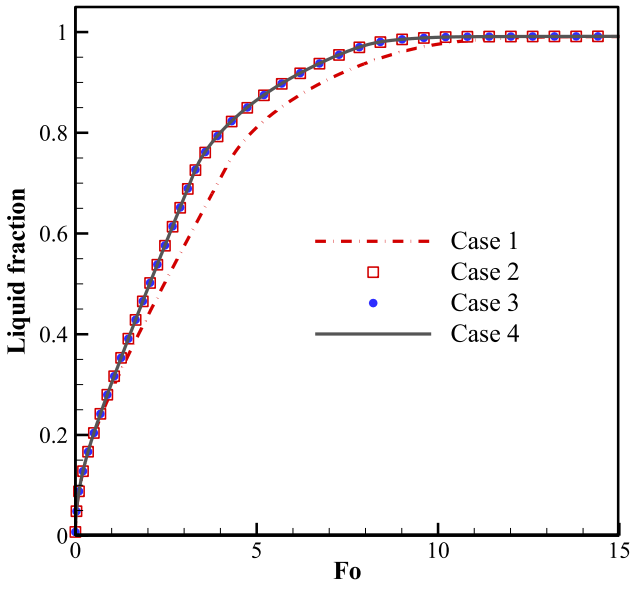

Fig. 2. The effect of the mesh size on the time-history of the liquid fraction.

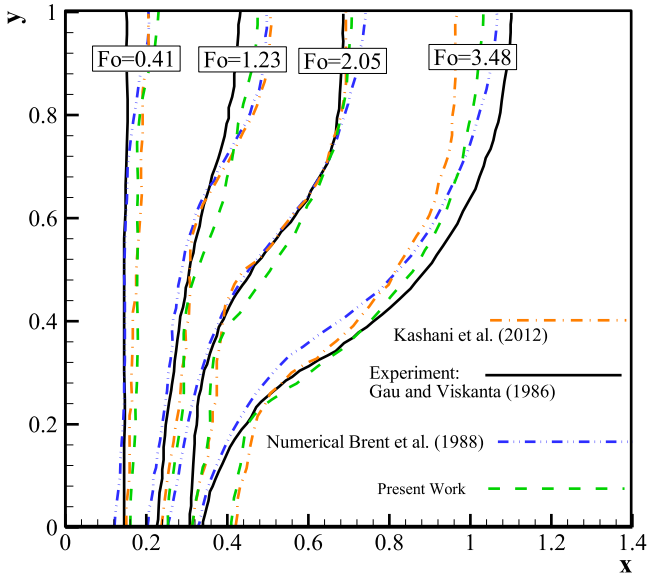

Fig. 3. Comparison of the melting interface between present work and the literature [33–35].

items corresponding to Table 1. As it is seen, with an increase in the number of the mesh nodes, the results are almost independent of the node number for case 2.

Ultimately, to validate the results, the numerical results of the current work are compared to the previous works [1, 33–35] for a simple fluid in a cavity. Fig. 3 represents a comparison of the melt interface in the present work with the previous works [33–35] in the absence of a magnetic-field. The experimental study conducted by Gau and Viskanta [33] reported on the role of natural convection heat transfer on the solid-liquid interface motion during

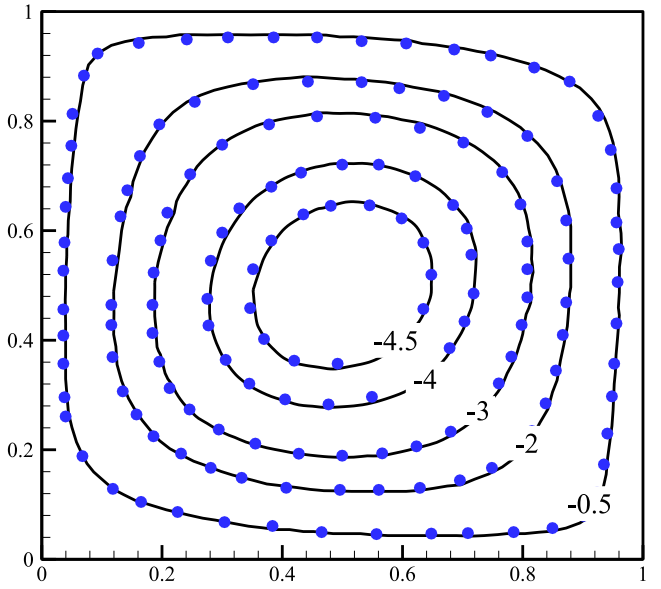

Fig. 4. Comparison between the streamlines of the present work (solid lines) and the literature (points) [36].

the melting process of a non-magnetic material. In their study, a rectangular enclosure with dimensions of 6.35 cm in width, 3.81 in depth, and 8.89 cm in height was considered as the test case, wherein, the vertical opposite walls were exposed to the heat source and heat sink. The utilized material in this experiment was Gallium with the melting point of 29.78 °C. This experiment can be represented as a non-dimensional cavity with an aspect ratio of 0.714 (height/width), Ra= 6×10^5, Pr = 0.0216, and Ste = 0.039. Fig. 4 reports the streamline in this research and that of [36] for the natural convection in the presence of a magnetic-field. The parameters for this validation are Ra = 10^5, Pr = 0.054, and Ha = 50. As can be seen in Figs. 3 and 4, the results of the current study make a good match to the previous studies and are appropriate to predict the melting process.

4. Results and discussions

The current work aims to address the simultaneous influence of two non-uniform magnetic-fields on the melting phase change in the presence of the free convection effects. The study parameters of the current work are the intensity ratio of two non-uniform magnetic-fields γ_r, Hartmann number Ha, and magnetic number Mn_f. The remaining parameters are retained fixed at Ste = 0.039, Pr = 0.021, Ra = 2.1×10^5, $Y_1 = 0.3$, $Y_2 = 0.7$, and Ec = 10^{-6}.

Fig. 5 shows the magnetic-fields applied to the melting process in different values of γ_r. As shown in Fig. 6, the effect of γ_r on the melting process in the cavity filled with PCM is examined as the first case. Fig. 6 illustrates the isothermal lines and the streamlines variations for the different Fourier number and γ_r. It is evident that by increasing the Fourier number the melting process proceeds, and the melted liquid region develops. The streamline patterns are entirely affected by the intensity variations of the two non-uniform magnetic-fields. With an increase in γ_r, the concentration of the magnetic-field lines in the top location of the cavity increases and weakens the streamlines as an inhibitor force against buoyancy forces. As a result, natural convection heat transfer reduces, slowing down the melting process. In other words, the concentration of the magnetic-field on the top of the cavity ($\gamma_r = 5$) increases the resistance against the natural convection flow, slowing down the melting process. Furthermore, for low Fourier numbers (Fo = 1), it can be seen that the isothermal lines are verti-

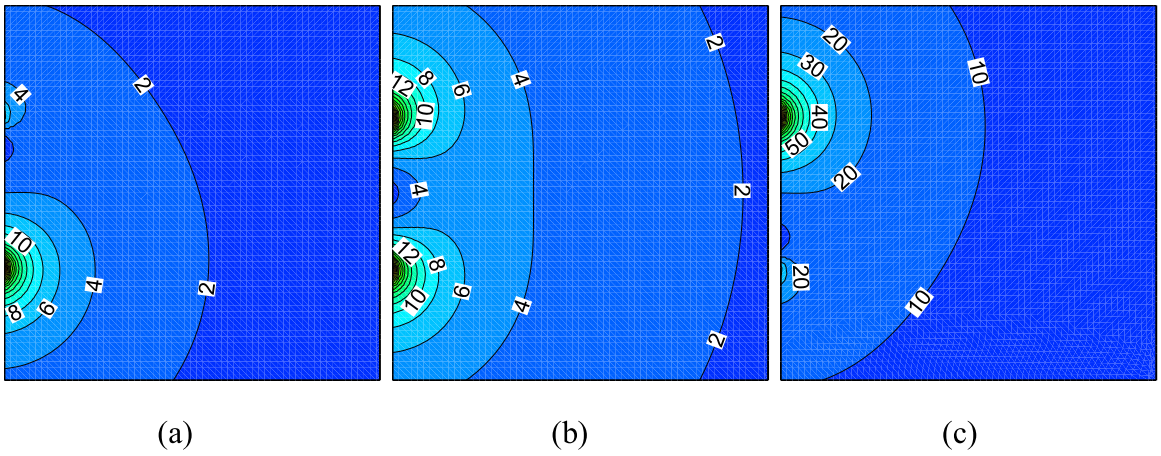

Fig. 5. The countours of magnetic fields applied on the charging process; (a) $\gamma_r = 0.2$, (b) $\gamma_r = 1$, and (c) $\gamma_r = 5$.

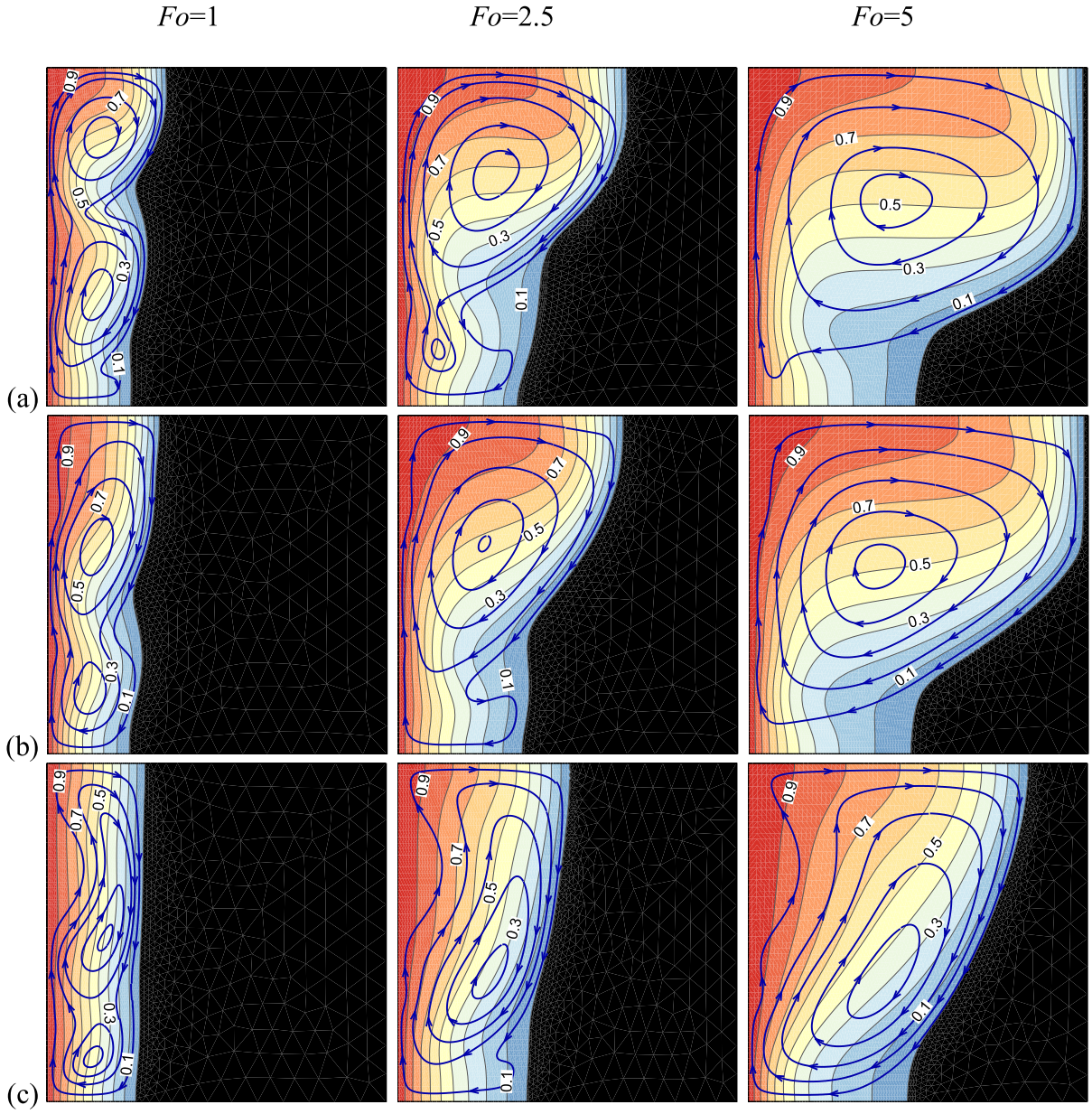

Fig. 6. The isothermal lines and the streamlines; (a) $\gamma_r = 0.2$, (b) $\gamma_r = 1$, and (c) $\gamma_r = 5$ inside melted PCM with respect to γ_r with passing non-dimensional time.

cal due to conduction prevailing over convection for all values of γ_r. The tendency of the isothermal lines to the horizontal position for higher values of Fourier numbers (Fo = 2.5, 5) indicates the domination of convection mode in the cavity. This tendency of the isothermal lines at the top of the cavity and near solid PCM reduces as γ_r increases, slowing down the charging of the thermal storage and PCM melting process. Column 3 (Fo = 5) demonstrates that the melting process at the lower area of the cavity is more influenced by conduction.

Fig. 7 presents the fraction of melted PCM versus Fo number for the different values of γ_r. It is completely clear that the diagram slope is very high for very at a low value of Fo, and the melting rate is high due to a lack of a notable thermal resistance between the warm surface and solid PCM. Thus, the melting proceeds with the same rate from there to almost Fo = 1.5. In this range, natural convection flow vortexes have no opportunity to grow, and conduction is dominant. Since the variables of γ_r do not affect conduction, increases in γ_r do not influence the melting process. After Fo = 1.5 and with the growth of flow vortices and prevailing of natural convection, reduction of melting diagram slope is observed with the increase in γ_r. The flow weakens as γ_r increases, and consequently, as thermal resistance, the

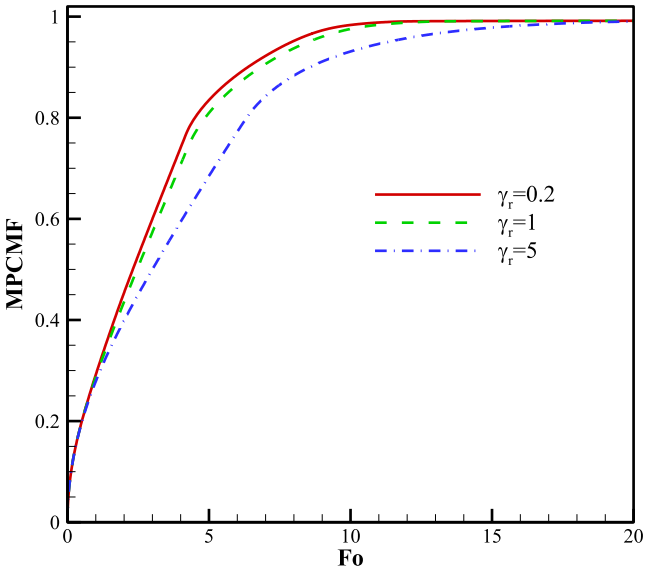

Fig. 7. The fraction of melted PCM with passing non-dimensional time for different γ_r.

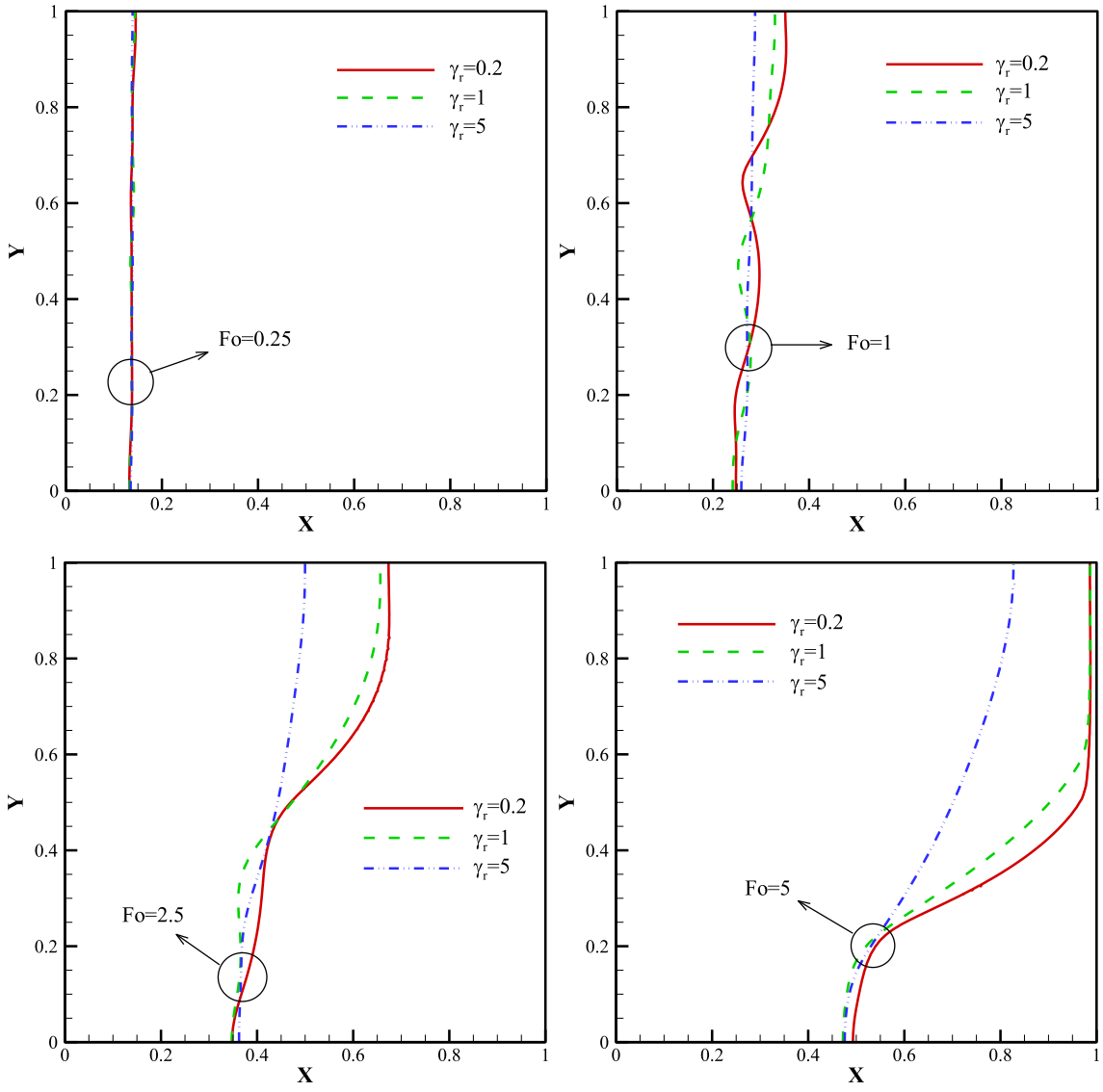

Fig. 8. The melting frontier at various non-dimensional time-steps for different γ_r.

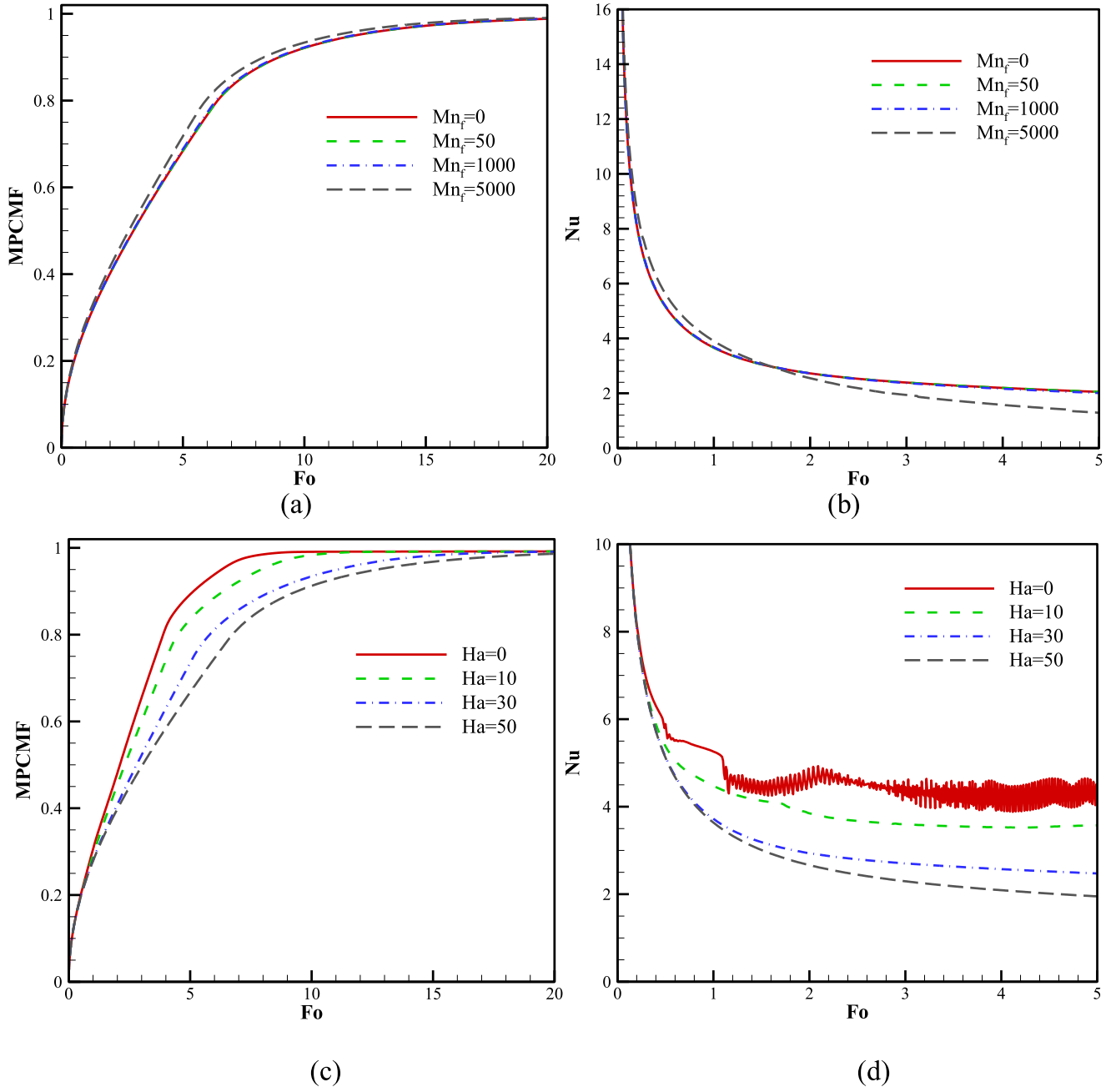

Fig. 9. The fraction of melted PCM and (b), (d) the average Nusselt number for (a), (b) different Mn_f ($\gamma_r = 1$ and $Ha = 30$) and (c), (d) Ha ($\gamma_r = 0.2$ and $Mn_f = 50$) with passing non-dimensional time.

melted PCM slows down heat transfer rate and thermal storage charging.

On the contrary, for $\gamma_r = 0.2$, since the thermal resistance reduces as natural convection increases, the diagram slope (red line) remains constant. Nevertheless, as the melted PCM volume increases, thermal resistance increases, reducing the diagram slope and melting rate (Fo = 5). Approximately at Fo = 17, with the majority of PCM melting, almost every four charts are placed on each other. Fig. 8 depicts the proceeding of the melting front boundary for various magnitudes of γ_r with passing the non-dimensional time. The variation of γ_r produces a minimal effect on the melted PCM region when Fo = 0.25. For higher Fourier number (i.e., Fo = 1, 2.5, 5), it is clear that the melted PCM increases as γ_r reduces. Fig. 8 shows that with increasing γ, the uniformity of the melting process increases. Therefore, it can be concluded that by strengthening the magnetic-field and applying more Lorentz and Kelvin forces at the top of the cavity, we can strengthen the uniformity of the melting process by weakening the buoyancy forces in this region.

Fig. 9 indicates the effects of an increase in magnetic and Hartmann numbers on melted PCM fraction and mean Nusselt number. The melted PCM fraction slightly increases as the magnetic number increases (Fig. 9a). As Fig. 9b indicates, the effects of Kelvin forces on fluid particles seem to change with time. These forces act to enhance buoyancy forces at Fo < 1.5; increasing mean Nusselt number. The fluctuation of Nusselt number in Fig. (9d) for the case of Ha=0 are due to the instability of natural convection flow. Indeed, by the reduction of Ha number, the fluid can more freely circulate in the cavity, and hence, it can also be more unstable. The trend of the behavior of Nu follows the trend of behavior for other Ha numbers.

On the contrary, for Fo < 1.5, the resistance against the buoyancy forces causes a reduction in mean Nusselt number. An increase in Hartmann number increases the inhibiting and resistant Lorentz force in fluid particles and reduces the melting process rate and mean Nusselt number. As shown, when Ha = 0, a quasi-steady state can be found at the end of the melting process.

5. Conclusion

The current work investigates the simultaneous effects of two non-uniform magnetic-fields on the melting phase change behavior of a PCM-filled cavity. The strengths of the magnetic-fields are not necessarily the same. The deformed mesh technique is employed to track the interface of molten liquid and solid portions of PCM. Galerkin finite element method, along with the Arbitrary Lagrangian-Eulerian is employed to integrate the governing equations. The mesh independence examination is carried out to ensure that the numerical results are independent of the number of elements. Comparisons between the results of the current work and the results reported in the literature confirm the validity of the computations and modeling.

The effects of governing parameters such as Hartman number Ha, Magnetic number Mn_f and the intensity ratio of two non-uniform magnetic-fields γ_r on the melting process are studied. The results show that the progress of the melting front completely depends on the intensity ratio of two non-uniform magnetic-fields γ_r. Besides, although the magnetic number has a slight effect on the melting, a raise in Hartman number can drastically decline the progressive of the melting front.

The results of the present study indicate the strong influence of the magnetic field on the control of the melting front. Hence, the optimization of the magnetic field as a case study for accurate control of melting/solidification can be subject to future studies.

Declaration of Competing Interest

None.

Supplementary materials

Supplementary material associated with this article can be found, in the online version, at doi:10.1016/j.ijheatmasstransfer.2019.119184.

References

[1] M. Sathiyamoorthy, A. Chamkha, Effect of magnetic field on natural convection flow in a liquid gallium filled square cavity for linearly heated side wall (s), Int. J. Therm. Sci. 49 (9) (2010) 1856–1865.
[2] A. Dogonchi, M. Sheremet, D. Ganji, I. Pop, Free convection of copper–water nanofluid in a porous gap between hot rectangular cylinder and cold circular cylinder under the effect of inclined magnetic field, J. Therm. Anal. Calorim. 135 (2) (2019) 1171–1184.
[3] J.C. Umavathi, S. Mohiuddin, M.A. Sheremet, MHD flow in a vertical channel under the effect of temperature dependent physical parameters, Chin. J. Phys. 58 (2019) 324–338.
[4] Y. Ma, R. Mohebbi, M. Rashidi, Z. Yang, M.A. Sheremet, Numerical study of MHD nanofluid natural convection in a baffled U-shaped enclosure, Int. J. Heat Mass Transfer 130 (2019) 123–134.
[5] N.S. Gibanov, M.A. Sheremet, H.F. Oztop, K. Al-Salem, MHD natural convection and entropy generation in an open cavity having different horizontal porous blocks saturated with a ferrofluid, J. Magn. Magn. Mater. 452 (2018) 193–204.
[6] C. Sivaraj, M. Sheremet, MHD natural convection and entropy generation of ferrofluids in a cavity with a non-uniformly heated horizontal plate, Int. J. Mech. Sci. 149 (2018) 326–337.
[7] C. Sivaraj, M.A. Sheremet, MHD natural convection in an inclined square porous cavity with a heat conducting solid block, J. Magn. Magn. Mater. 426 (2017) 351–360.
[8] S. Mehryan, M.A. Sheremet, M. Soltani, M. Izadi, Natural convection of magnetic hybrid nanofluid inside a double-porous medium using two-equation energy model, J. Mol. Liq. 277 (2019) 959–970.
[9] Z. Li, M. Sheikholeslami, A.J. Chamkha, Z. Raizah, S. Saleem, Control volume finite element method for nanofluid MHD natural convective flow inside a sinusoidal annulus under the impact of thermal radiation, Comput. Methods Appl. Mech. Eng. 338 (2018) 618–633.
[10] S. Mehryan, M. Izadi, A.J. Chamkha, M.A. Sheremet, Natural convection and entropy generation of a ferrofluid in a square enclosure under the effect of a horizontal periodic magnetic field, J. Mol. Liq. 263 (2018) 510–525.
[11] A.J. Chamkha, M. Al-Amin, A. Aly, Unsteady double-diffusive natural convective MHD flow along a vertical cylinder in the presence of chemical reaction, thermal radiation and Soret and Dufour effects, J. Naval Archit. Mar. Eng. 8 (1) (2011) 25–36.
[12] A.J. Chamkha, A. Rashad, Unsteady heat and mass transfer by MHD mixed convection flow from a rotating vertical cone with chemical reaction and Soret and Dufour effects, Can. J. Chem. Eng. 92 (4) (2014) 758–767.
[13] B. Mallikarjuna, A. Rashad, A.J. Chamkha, S.H. Raju, Chemical reaction effects on MHD convective heat and mass transfer flow past a rotating vertical cone embedded in a variable porosity regime, Afrika Matematika 27 (3–4) (2016) 645–665.
[14] N.H. Boukani, A. Dadvand, A.J. Chamkha, Melting of a nano-enhanced phase change material (NePCM) in partially-filled horizontal elliptical capsules with different aspect ratios, Int. J. Mech. Sci. 149 (2018) 164–177.
[15] N.S. Bondareva, M.A. Sheremet, Conjugate heat transfer in the PCM-based heat storage system with finned copper profile: application in electronics cooling, Int. J. Heat Mass Transfer 124 (2018) 1275–1284.
[16] N.S. Bondareva, B. Buonomo, O. Manca, M.A. Sheremet, Heat transfer performance of the finned nano-enhanced phase change material system under the inclination influence, Int. J. Heat Mass Transfer 135 (2019) 1063–1072.
[17] M. Ghalambaz, T. Groşan, I. Pop, Mixed convection boundary layer flow and heat transfer over a vertical plate embedded in a porous medium filled with a suspension of nano-encapsulated phase change materials, J. Mol. Liq. 293 (2019) 111432.
[18] M. Ghalambaz, A.J. Chamkha, D. Wen, Natural convective flow and heat transfer of nano-encapsulated phase change materials (NEPCMs) in a cavity, Int. J. Heat Mass Transfer 138 (2019) 738–749.
[19] K.A. Ayoubloo, M. Ghalambaz, T. Armaghani, A. Noghrehabadi, A.J. Chamkha, Pseudoplastic natural convection flow and heat transfer in a cylindrical vertical cavity partially filled with a porous layer, Int. J. Numer. Methods Heat Fluid Flow (2019).
[20] R.Y. Farsani, A. Raisi, A.A. Nadooshan, S. Vanapalli, The effect of a magnetic field on the melting of gallium in a rectangular cavity, Heat Transfer Eng. 40 (1–2) (2019) 53–65.
[21] M. Sheikholeslami, O. Mahian, Enhancement of PCM solidification using inorganic nanoparticles and an external magnetic field with application in energy storage systems, J. Clean. Prod. 215 (2019) 963–977.
[22] M. Sheikholeslami, Solidification of NEPCM under the effect of magnetic field in a porous thermal energy storage enclosure using CuO nanoparticles, J. Mol. Liq. 263 (2018) 303–315.
[23] F. Selimefendigil, H.F. Oztop, A.J. Chamkha, Natural convection in a CuO–water nanofluid filled cavity under the effect of an inclined magnetic field and phase change material (PCM) attached to its vertical wall, J. Therm. Anal. Calorim. 135 (2) (2019) 1577–1594.
[24] M. Sheikholeslami, K. Vajravelu, Nanofluid flow and heat transfer in a cavity with variable magnetic field, Appl. Math. Comput. 298 (2017) 272–282.
[25] M. Izadi, R. Mohebbi, A.A. Delouei, H. Sajjadi, Natural convection of a magnetizable hybrid nanofluid inside a porous enclosure subjected to two variable magnetic fields, Int. J. Mech. Sci. 151 (2019) 154–169.
[26] M. Sheikholeslami, T. Hayat, A. Alsaedi, Numerical study for external magnetic source influence on water based nanofluid convective heat transfer, Int. J. Heat Mass Transfer 106 (2017) 745–755.
[27] M. Sheikholeslami, H.B. Rokni, Numerical modeling of nanofluid natural convection in a semi annulus in existence of Lorentz force, Comput. Methods Appl. Mech. Eng. 317 (2017) 419–430.
[28] M. Sheikholeslami, M. Seyednezhad, Nanofluid heat transfer in a permeable enclosure in presence of variable magnetic field by means of CVFEM, Int. J. Heat Mass Transfer 114 (2017) 1169–1180.
[29] M. Ghalambaz, S.M.H. Zadeh, S. Mehryan, I. Pop, D. Wen, Analysis of melting behavior of PCMs in a cavity subject to a non-uniform magnetic field using a moving grid technique, Appl. Math. Model. 77 (2020) 1936–1953.
[30] J.N. Reddy, An introduction to the finite element method, New York, (1993).
[31] J.N. Reddy, D.K. Gartling, The Finite Element Method in Heat Transfer and Fluid Dynamics, CRC Press, 2010.
[32] O.C. Zienkiewicz, R.L. Taylor, P. Nithiarasu, The finite element method for fluid dynamics, The Finite Element Method for Fluid Dynamics, 7th edition, ButterworthHeinemann, Oxford, 2014.
[33] C. Gau, R. Viskanta, Melting and solidification of a pure metal on a vertical wall, J. Heat Transfer 108 (1) (1986) 174–181.
[34] S. Kashani, A. Ranjbar, M. Abdollahzadeh, S. Sebti, Solidification of nano-enhanced phase change material (NEPCM) in a wavy cavity, Heat Mass Transfer 48 (7) (2012) 1155–1166.
[35] A. Brent, V. Voller, K. Reid, Enthalpy-porosity technique for modeling convection-diffusion phase change: application to the melting of a pure metal, Numer. Heat Transfer Part A Appl. 13 (3) (1988) 297–318.
[36] M. Sathiyamoorthy, A.J. Chamkha, Natural convection flow under magnetic field in a square cavity for uniformly (or) linearly heated adjacent walls, Int. J. Numer. Methods Heat Fluid Flow 22 (5) (2012) 677–698.